

Dalton Transactions

Accepted Manuscript



This is an *Accepted Manuscript*, which has been through the Royal Society of Chemistry peer review process and has been accepted for publication.

Accepted Manuscripts are published online shortly after acceptance, before technical editing, formatting and proof reading. Using this free service, authors can make their results available to the community, in citable form, before we publish the edited article. We will replace this *Accepted Manuscript* with the edited and formatted *Advance Article* as soon as it is available.

You can find more information about *Accepted Manuscripts* in the [Information for Authors](#).

Please note that technical editing may introduce minor changes to the text and/or graphics, which may alter content. The journal's standard [Terms & Conditions](#) and the [Ethical guidelines](#) still apply. In no event shall the Royal Society of Chemistry be held responsible for any errors or omissions in this *Accepted Manuscript* or any consequences arising from the use of any information it contains.



This paper reports the synthesis of novel photocatalysts consisting of TiO_2 nanoparticles and glass fibres (GF) using a two-step process. The method involves the hydrolysis of titanium tetrachloride in the presence of GF and a following hydrothermal process in alkali condition. Various techniques are employed to characterize the morphology, structure and crystallinity of TiO_2 on fibre surface. The results show that depending on the experiment setups, TiO_2 nanoparticles exhibit spherical or flake-like morphology, forming characteristic hierarchical structures along with flexible GF. Flake-like TiO_2/GF exhibits much enhanced photocatalytic activity thanks to the large surface area and hetero-junction of anatase and $\text{TiO}_2\text{-B}$ phases observed in its structure. An interesting observation is that the alkali treatment of GF leads to the formation of porous structures on fibre surface, facilitating the adsorption-concentration-promoted photocatalytic process. The removal ratio of organic dye by employing TiO_2/GF remains more than 80% after six cyclic runs, showing the reusability of photocatalysts in real application. The novelty of this work lies in the synergy arising from materials with unique morphologies, structures and availabilities as well as capabilities in separating photogenerated electron-hole pairs, which have not been specifically considered previously in photocatalytic semiconductors.

Controlled synthesis of hierarchical TiO₂ nanoparticles on glass fibres and their photocatalytic performance

Lin Chen^{a, c}, Sudong Yang^{a, b}, Edith Mäder^d, Peng-Cheng Ma^{a, b, *}

^aLaboratory of Environmental Science and Technology, The Xinjiang Technical Institute of Physics and Chemistry, Chinese Academy of Sciences, Urumqi 830011, China

^bKey Laboratory of Functional Materials and Devices for Special Environments, Chinese Academy of Sciences, Urumqi 830011, China

^cGraduate University of Chinese Academy of Science, Beijing 100049, China

^dLeibniz Institute of Polymer Research Dresden, Hohe Street 6, Dresden 01069, Germany

* Corresponding author. Tel: +86-991-6992225; E-mail: mapc@ms.xjb.ac.cn (PC Ma).

Abstract

This paper reports the synthesis of novel photocatalysts consisting of TiO₂ nanoparticles and glass fibres (GF) using a two-step process. The method involves the hydrolysis of titanium tetrachloride in the presence of GF and a following hydrothermal process in alkali condition. Various techniques are employed to characterize the morphology, structure and crystallinity of TiO₂ on fibre surface. The results show that depending on the experiment setups, TiO₂ nanoparticles exhibit spherical or flake-like morphology, forming characteristic hierarchical structures along with flexible GF. Flake-like TiO₂/GF exhibits much enhanced photocatalytic activity thanks to the large surface area and hetero-junction of anatase and TiO₂-B phases observed in its structure. An interesting observation is that the alkali treatment of GF leads to the formation of porous structures on fibre surface, facilitating the adsorption-concentration-promoted photocatalytic process. The removal ratio of organic dye by employing TiO₂/GF remains more than 80% after six cyclic runs, showing the reusability of photocatalysts in real application. The novelty of this work lies in the synergy arising from materials with unique morphologies, structures and availabilities as well as capabilities in separating photogenerated electron-hole pairs, which have not been specifically considered previously in photocatalytic semiconductors.

1. Introduction

Semiconductor photocatalysis represents an emerging area in environmental catalysis with significant potential to detoxify noxious organic pollutants in an effective manner.^{1,2} Among different photocatalysts, titanium dioxide (TiO₂) is one of the most widely applied materials for the mineralization of organic materials and photocatalytic hydrogen production from water because of its stability, non-toxicity, availability, cost-effectiveness, as well as ability to efficiently degrade a variety of harmful organic materials in aqueous systems.³⁻⁵ In particular, nanosized TiO₂ has attracted considerable attention in photocatalytic applications due to its unique properties such as quantum confinement and high surface to volume ratio.⁶ Unfortunately, like other nanomaterials, TiO₂ nanoparticles tend to aggregate in suspension, leading to a rapid loss in active sites and photocatalytic capability.⁷⁻⁸ In addition, the post separation and recycle of TiO₂ nanoparticles in a slurry system pose a key obstacle for their practical applications. These drawbacks have led to a number of attempts to find suitable supports, on which TiO₂ nanoparticles can be anchored chemically or mechanically, for various photocatalytic reactions. Spherical silica and alumina particles, mineral clay, activated carbon, have been applied to fulfill this purpose with varying degree of success.⁹⁻¹¹ Glass fibre (GF), a material consisting of numerous extremely fine fiber of glass, appears to be a promising candidate to achieve this goal thanks to its high aspect ratio, excellent flexibility, light weight, low cost, transparency for natural light and stability against ultraviolet rays.¹²⁻¹⁴ Deposition of TiO₂ onto GF has proven to be an effective method to avoid the severe agglomeration of nanoparticles and maintain their photocatalytic activities. You et al¹⁵ used a sol-gel method to coat TiO₂ nanoparticles with uniform size on GF, and the composites exhibited enhanced capability for the photocatalytic degradation of toluene. Yu et al adopted a liquid phase deposition method to anchor anatase TiO₂ nanoparticles on GF and observed a lower deactivation rate for the photocatalytic oxidation of nitrogen monoxide.¹⁶

However, successful deposition of TiO₂ on GF surface is a challenging job because of low surface area of the support and weak interactions between the fibres and nanoparticles. For example, when GF was immersed into a TiO₂ sol at 90 °C for 2 h, only about 25% of fibre surface was covered by TiO₂ nanoparticles.¹⁷ While this deposition process can be optimized by applying a thin layer of epoxy as an adhesive on GF surface, it may bring negative effect on the semiconducting properties of TiO₂ nanoparticles. In addition, there is a concern that the crystallinity of in-situ generated TiO₂ nanoparticles may be affected by the presence of heterogeneous glass material, and this issue has not been considered in previous studies so far. Therefore, the development of a facile technique that can maintain a high surface area and excellent photocatalytic properties of TiO₂ on GF is desirable.

This paper is a part of a larger project in developing materials with hierarchical structures for environmental remediation. Herein, we reported the preparation of photocatalysts consisting of microscale glass fibres and nanoscale TiO₂ nanoparticles with controlled morphologies and crystal structures, aiming at enhancing the photocatalytic capability of material and stabilizing this property under cyclic runs. The morphology, surface information and crystallinity of TiO₂ on fibre surface were studied, and the photocatalytic activity of composites was evaluated.

2. Experiment

2.1 Materials

E-glass fibres with an average diameter of 12 μm were spun at the Leibniz Institute of Polymer Research Dresden, producing a yarn containing 204 filaments. Titanium tetrachloride (TiCl_4 , 98%), ammonium sulfate ($(\text{NH}_4)_2\text{SO}_4$), sulfuric acid (96%, H_2SO_4), ammonia water (28%, $\text{NH}_3\cdot\text{H}_2\text{O}$), sodium chloride (NaCl), hydrochloric acid (37%, HCl), methyl orange (MO) were purchased from Tianjing Chemical Company, China. All of these chemical reagents were of analytical grade and used without further purification. Ultrapure water (Millipore, resistivity $> 18.5 \text{ M}\Omega\cdot\text{cm}$) was used in all experiments.

2.2 Synthesis of $\text{TiO}_2/\text{glass fibre (TiO}_2/\text{GF)}$ photocatalysts

Figure 1 shows the experimental setups for the preparation of TiO_2/GF photocatalysts. In a typical process, 1.5 g $(\text{NH}_4)_2\text{SO}_4$ was slowly added into 100 mL of sulfuric acid (0.01 M) and stir for 5 minutes. Then 1 mL of TiCl_4 was added dropwise into the mixture under an ice water bath. This was followed by the introduction of 0.5 g GF into the system and heated to 95 $^\circ\text{C}$. The mixture was kept at this temperature for 3 h, producing GF decorated with spherical TiO_2 nanoparticles (Step I in Figure 1). The sample was separated from the liquid media by filtration, followed by washing with water and ethanol for several times and dried in a vacuum oven at 60 $^\circ\text{C}$ for 3 h.

GF with flake-like TiO_2 nanoparticles (Step II in Figure 1) was prepared by processing spherical TiO_2/GF (Produced in Step I) under alkali condition. Briefly, 0.5 g spherical TiO_2/GF was added into 60 mL aqueous ammonia with 0.4 M concentrations of NaCl , followed by a hydrothermal treatment in an autoclave at 150 $^\circ\text{C}$ for 12 h, yielding titanate/GF. Then the sample was washed with 0.1 M HCl and water for several times and calcined at 350 $^\circ\text{C}$ for 2 h, producing flake-like TiO_2/GF . For comparison, flake-like TiO_2 powder was also made by using spherical TiO_2 nanoparticles without GF while other synthetic conditions were kept the same.

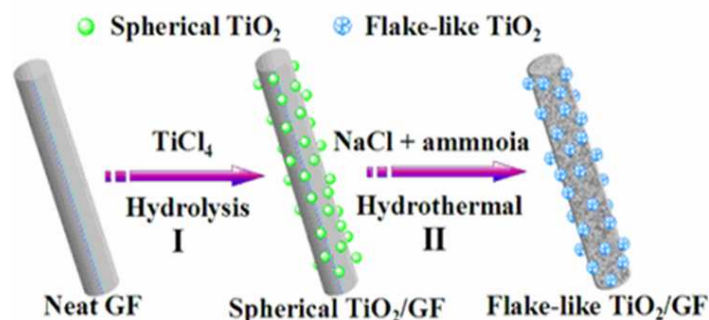


Figure 1. Schematics showing the preparation of hierarchical TiO_2/GF photocatalysts.

2.3 Evaluation on the photocatalytic activity of materials

The photocatalytic performance of samples was evaluated using a rectangular double-walled reactor made from quartz, and the solution to be degraded was placed in its inner part. The reactor was equipped with inlet and outlet of water so that the heating effect to the solution due to the UV light can be minimized during the photocatalytic reaction. Irradiation was provided by a 500 W high-pressure mercury lamp with a major emission at 365 nm, located in the center of reactor. A magnetic stirrer was employed at the bottom of the reactor to avoid the precipitation of photocatalysts in solution. The photocatalytic activity of samples was evaluated by measuring the degradation ratio of organic dye, MO, at room temperature. The initial concentration of MO was $20 \text{ mg}\cdot\text{L}^{-1}$, and the loading of photocatalyst in solution was kept at 0.2 g per 100 mL of MO solution. The UV light irradiated perpendicularly to the surface of suspension and the distance between the lamp and the surface of dye solution was kept constantly at 10 cm. For the evaluation of photocatalytic activity of material, the sample was stirred at first in MO solution in the dark for 40 min to reach adsorption equilibrium, then a mercury lamp was employed to start the photocatalytic reaction. A certain amount of solution was collected at different time (0-80 min), and the concentration of MO in solution was determined by measuring the absorbance at 465 nm (maximum absorption)³¹ using a UV-Vis spectrophotometer (Shimadzu UV-2550). The degradation efficiency was defined as follows:¹⁸

$$\text{Degradation}(\%) = \left(1 - \frac{C}{C_0}\right) \times 100\% \quad (1)$$

where C_0 is the concentration of MO at adsorption equilibrium, and C is the residual concentration of MO at varying intervals of UV irradiation. The kinetics of photodegradation was studied using a pseudo first-order principle, as expressed in Eq. 2:²⁰

$$\ln\left(\frac{C_0}{C}\right) = k \cdot t \quad (2)$$

where k is the degradation rate (min^{-1}), and t is the time of photocatalytic reaction (min).

Free radicals produced during the photocatalytic reaction were characterized by a fluorescence method using terephthalic acid (TA) as a probe molecule.¹⁹ In brief, 100 mg photocatalyst was dispersed in 200 mL solution consisting of TA ($5 \times 10^{-4} \text{ M}$)

and NaOH (2×10^{-3} M). The resulting suspension was exposed to UV light, and 5 mL of the suspension was collected at different intervals and centrifuged to measure the maximum fluorescence intensity with an excitation wavelength of 320 nm. To verify the main active species generated in the photocatalysts, experiments were performed in above photocatalytic degradation system by adding isopropanol (IPA), ammonium oxalate (AO) and benzoquinone (BQ) as trapping agents.²⁰

2.4 Characterization

Various techniques were employed to characterize the photocatalyst. X-ray powder diffraction (XRD) and transmission electron microscopy (TEM) were used to characterize the changes in structure, crystallinity and chemical information of samples. XRD patterns were recorded using a diffractometer (Bruker-D8) equipped with a Cu K_{α} radiation source ($\lambda = 0.154$ nm). TEM images (JEOL-JEM 2100) were obtained by observing the sample at an acceleration voltage of 200 kV. A scanning electron microscope (SEM, Zeiss Supra55VP) was employed to exam the morphology of fibres at different steps. Surface area and porosity of samples were measured using a surface area analyzer (Micromeritics ASAP 2020) based on the Brunauer-Emmett-Teller (BET) theory and Barrett-Joyner-Halenda (BJH) method, respectively. The phase of TiO₂ on GF surface was verified on a Raman spectrometry (WITec ALPHA 300M). The content of TiO₂ on fibre surface was analyzed by dissolving the sample with HNO₃ and HF, and the concentration of metal ions was determined by an induced coupling plasma-atomic emission spectrometry (ICP-AES, Optima-7000DV). UV-Vis diffuse reflectance spectrometry was performed on a spectrophotometer (SOLID 3700, Shimadzu) over the wavelength range of 200-800 nm.

3. Results and discussion

3.1 Structure and morphology of photocatalysts

Crystal structures of photocatalysts were characterized by XRD. The samples exhibit distinctive diffraction patterns as shown in Figure 2, revealing the different crystallinity of TiO₂ on GF surface. For spherical TiO₂/GF sample, characteristic peak (26.1°) attributed to anatase TiO₂ is observed (Figure 2a), suggesting the in-situ formation of TiO₂ by a simple hydrolysis using TiCl₄ as titanium source in the presence of GF.²¹ The intensity of TiO₂ diffraction peaks were relatively weak possibly due to the superposition on the wide bands associated with the silica phase of GF. The precursor of flake-like TiO₂/GF, i.e., titanate/GF, shows diffraction peak at about $2\theta = 9.7^{\circ}$ (Figure 2b), assigned to the (200) crystal face of layered titanate.²² In addition, two weak peaks at 25.3° and 48.1° appear, which are attributed to the transformation from titanate to anatase TiO₂ by partly dehydration during the drying process. However, when titanate/GF was processed at 350°C for 2 h to produce flake-like TiO₂/GF, the titanate phase at 9.7° disappears in the XRD pattern (Figure 2c), suggesting the phase change of titanate.

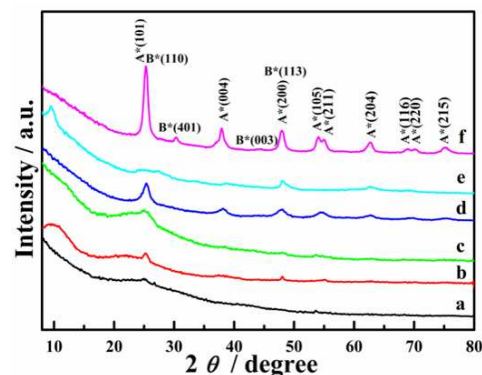


Figure 2. XRD patterns of photocatalysts and corresponding precursors (a: spherical TiO₂/GF; b: titanate/GF; c: flake-like TiO₂/GF; d: spherical TiO₂; e: titanate; f: flake-like TiO₂).

To further verify the crystallinity of TiO₂ on fibre surface, the catalysts were prepared as powders without GF. In the first hydrolysis step (Figure 2d), anatase TiO₂ was identified ($2\theta = 25.4^{\circ}, 38.0^{\circ}, 48.1^{\circ}, 53.8^{\circ}, 55.0^{\circ}, 62.8^{\circ}, 68.8^{\circ}, 70.5^{\circ}, 75.0^{\circ}$ for (101), (004), (200), (105), (211), (204), (116), (220), (215) planes of anatase, respectively, JCPDS No.21-1272).²¹ After alkali hydrothermal process, layered titanate ($\text{H}_2\text{Ti}_2\text{O}_5 \cdot \text{H}_2\text{O}$) structure was confirmed by the corresponding JCPDS file No. 47-0124 ($2\theta = 25.3^{\circ}, 27.8^{\circ}, 24^{\circ}, 39^{\circ}, 48^{\circ}$ for (200), (310), (110), (501), (020) planes, respectively),²² as shown in Figure 2e. In the patterns of samples after calcination (i.e., flake-like TiO₂), diffraction peaks attributed to titanate disappears and peaks attributed to anatase appear at $2\theta = 25.3^{\circ}, 37.8^{\circ}, 48.0^{\circ}, 53.1^{\circ}, 55.4^{\circ}, 62.7^{\circ}$ (Figure 1f). Besides these anatase peaks (A^* in Figure 2f), a new phase named TiO₂-B, a metastable interphase between $\text{H}_2\text{Ti}_2\text{O}_5 \cdot \text{H}_2\text{O}$ and anatase, appears in the flake-like TiO₂ sample. Its diffraction peaks can be found at $24.9^{\circ}, 29.5^{\circ}, 33.3^{\circ}, 43^{\circ}, 44.2^{\circ}, 48.6^{\circ}$ and 58.4° (B^* in Figure 1f), corresponding to the $d_{110}, d_{002}, d_{311}, d_{003}, d_{601}, d_{113}$ and d_{711} of TiO₂-B (JCPDS No. 74-1940).²³ The unique diffraction peaks at 29.8° and 44.2° represents the (401) and (003) planes of TiO₂-B, respectively, while all other major TiO₂-B diffraction peaks overlap with those arising from anatase phase, for example, diffraction peaks of TiO₂-B (110) at 24.9° and (113) at 48.6°

overlap with anatase (101) at 25.1° and (101) at 48.1° .²⁴ It should be emphasized here that the intensity of diffraction peaks found in TiO_2 powders are significantly higher than those from TiO_2/GF , confirming the assumption that signals arising from GF overlap these from TiO_2 on fibre surface.

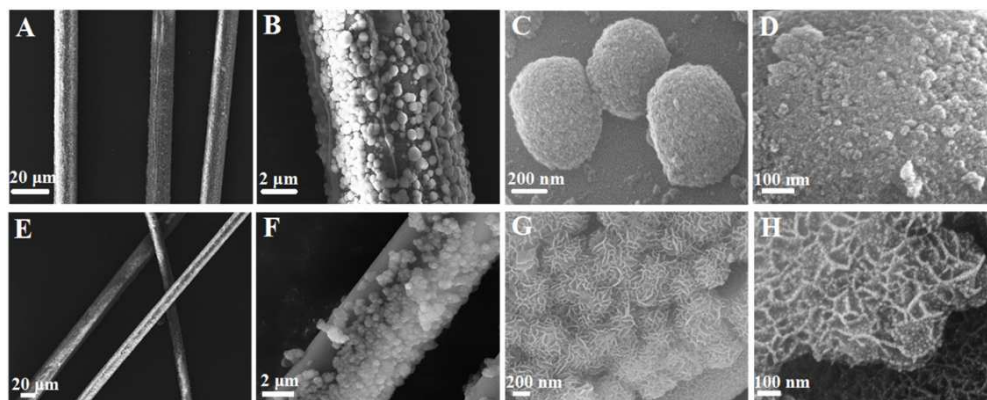


Figure 3. SEM images showing the morphology of photocatalysts prepared at different steps (A-D: Spherical TiO_2/GF ; E-H: Flake-like TiO_2/GF).

Morphological analysis of photocatalysts was performed in order to study the features of TiO_2 particles on fibre surface. Figure 3 shows typical SEM images of samples under different magnifications. A homogeneous distribution of sphere with size ranging from 400 to 500 nm was observed in the spherical TiO_2/GF sample (A-C in Figure 3). A close observation shows that these particles consist of fine particles in nanometer scale (Figure 3D). In sharp contrast, the flake-like TiO_2/GF sample exhibits the attachment of dense particles on fibre surface (E and F in Figure 3), and these particles retain the original spherical morphology of TiO_2 precursor. Higher magnification images (G and H in Figure 3) show that the microstructure of TiO_2 particles changed from spherical to flake-like one after alkali treatment, forming hierarchical structures consisting of flower-like structure in microscale and packed nanoplates in nanoscale. These nanoplates are aligned perpendicularly to the fibre surface with clear layer structures. The reason for this observation is the formation of titanate on fibre surface. It was reported that layered titanates can be constructed by stacking anionic TiO_2 manolayers with the counter cations (NH_4^+ or Na^+),²⁵ and this process can be favored under alkali condition, like the pH value of 12 employed in this study. Anatase TiO_2 and titanate contain zigzag ribbons of TiO_6 octahedra that share four edges with others, and this structural similarity makes NH_4^+ and water molecules penetrate into the anatase phase, resulting in the formation of titanate easily. Therefore, the original spherical morphology of TiO_2 on fibre surface produced in Step I can be retained largely in flake-like TiO_2/GF . When the layered titanate was calcined at elevated temperature, the deintercalation of NH_4^+ and water from the interlayer rearranges the structure of titanate from layer one to tetragonal lattice, resulting in the generation of flake-like TiO_2 structures on fibre surface as well as appearance of new phase $\text{TiO}_2\text{-B}$.^{26,27} ICP results reveal that as-synthesized spherical TiO_2 and flake-like TiO_2 accounted for 10 %, 8.9 % of total mass of photocatalysts, respectively.

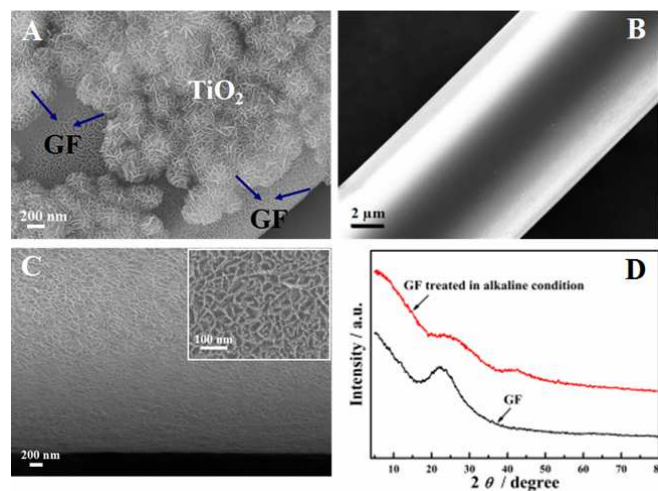


Figure 4. Effect of alkali treatment on the morphology of GF (A: flake-like TiO_2/GF ; B: pristine GF; C: GF treated with alkali; D: corresponding XRD pattern of GF before and after alkali treatment).

Besides the morphological change of TiO₂ nanoparticles on fibre surface, an interesting observation is that the alkali treatment of spherical TiO₂/GF leads to the formation of porous nanostructures on fibre surface (arrows in Figure 4A), pretty similar to that of hydrotalcite materials.²⁸ To reveal the mechanism behind this, comparative experiments were conducted using pristine GF under the same hydrothermal condition without titanium source. The results show that pristine GF exhibits a smooth surface (Figure 4B). After hydrothermal treatment in aqueous ammonia (pH=12.0), the surface becomes rougher and irregular (Figure 4C), characteristic nanosheets are identified (Inset in Figure 4B), providing direct evidence that the formation of this structure is dominated by alkali ions other than the titanium compounds. It is known that E-type GF contains metal ions like Ca²⁺, Mg²⁺ and Al³⁺, and these ions can be transformed to corresponding hydroxide compounds to form agglomerated platelet-shaped particles via co-precipitation route under alkaline condition. This explanation is supported partly by the XRD patterns of GF before and after alkali treatment (Figure 4D): pristine GF mainly has one broad peak at 22° (2θ), whereas the treated one by alkali exhibits characteristic diffraction peaks representing (00l) harmonics at low angle, pretty similar to that of layered double hydroxides (LDH) material, a compound comprise an unusual class of layered materials with charged layers and weak bonds.²⁹⁻³² It is worth mentioning that the numerous nanopores observed on GF surface may increase the surface area of photocatalyst, facilitating the physical adsorption of organic materials in liquid media.

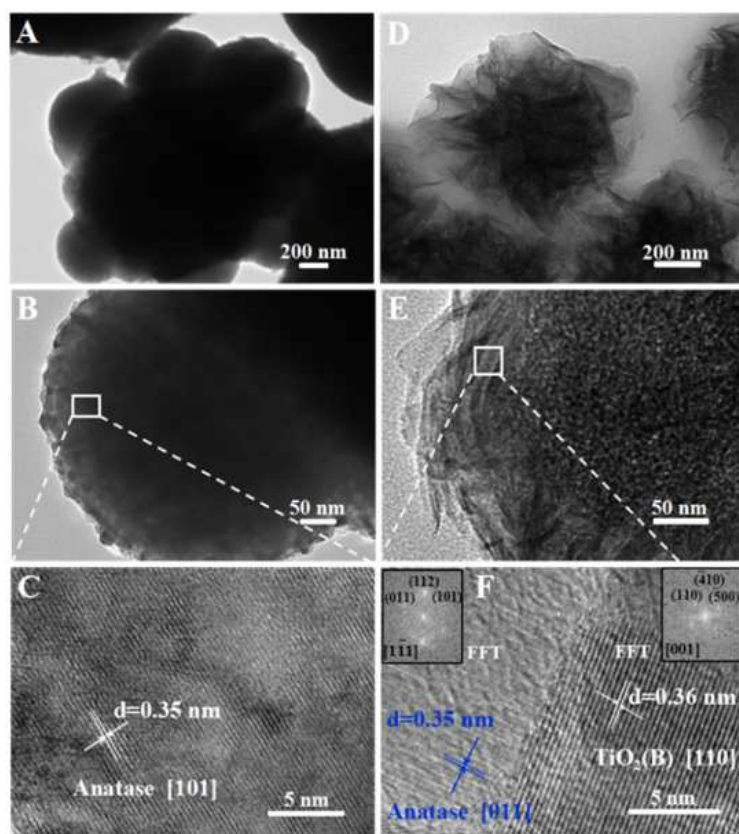


Figure 5. TEM images showing the morphology and crystallinity of TiO₂ on fibre surface (A-C: Spherical TiO₂/GF; D-F: Flake-like TiO₂/GF).

The general morphology and crystallinity of TiO₂ on fibre surface were characterized using high resolution TEM as a complementary technique. The prepared photocatalysts exhibit spherical and flake-like TiO₂ nanostructures (A and D in Figure 5), which are consistent with SEM results. The TEM image in Figure 5B reveals that the spherical TiO₂ possesses wormhole-like mesopores which are well dispersed in the entire sphere, whereas the one recorded from the edge of flake-like TiO₂ (Figure 5E) shows that surface of hierarchical TiO₂ nanostructures is actually made of interconnected ultrathin nanosheets with several layers. The interlayer spacing of these nanosheets is several nanometers. High resolution TEM image shows that spherical TiO₂ nanoparticles consists of crystal with fringe spacing of 0.35 nm (Figure 5C), corresponding to the (101) plane of anatase phase. In contrast, the flake-like TiO₂ shows two distinct regions (Figure 5F): i) The left side with lattice spacing of 0.35 nm, corresponding to the (101) plane of anatase TiO₂; and ii) The right side with lattice spacing of 0.36 nm, representing the (110) plane of TiO₂-B phase.³³ The crystal lattice directions of two phases are different, resulting in an obvious interface. Therefore, it can be confirmed that hetero-junction with anatase and TiO₂-B phases were formed in the flake-like TiO₂. Further characterization using fast Fourier transform (FFT) (Inset in Figure 5F) shows that the orientations of

anatase and TiO₂-B phases are [011] and [110], respectively.

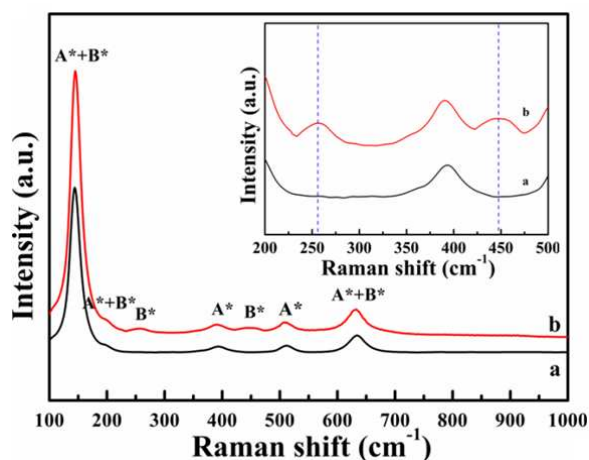


Figure 6. Raman spectra of spherical TiO₂/GF (a); flake-like TiO₂/GF (b).

Raman spectrometry is a powerful technique to get the phase composition of TiO₂, and the vibration of -Ti-O-Ti- has been well documented in literature.³⁴ Figure 6 shows the Raman spectra of TiO₂/GF photocatalyst. For simplicity, the peaks attributed to the anatase phase of TiO₂ are labeled as A* and those of TiO₂-B are labeled as B*. The sample containing spherical TiO₂ displays typical anatase Raman bands at 144 cm⁻¹(E_g), 197 cm⁻¹(E_g), 392 cm⁻¹(B_{1g}), 513 cm⁻¹(A_{1g}+B_{1g}) and 636 cm⁻¹(E_g). After hydrothermal process, two new peaks at 256 and 450 cm⁻¹ appear, suggesting the existence of TiO₂-B phase in the flake-like TiO₂/GF. The nonoverlapping diagnostic bands along with others attributed to the anatase phase (Inset in Figure 6) indicate that the flake-like TiO₂ on fibre surface indeed possessed a mixed phase structures, which are quite agreeable with XRD and TEM analysis.

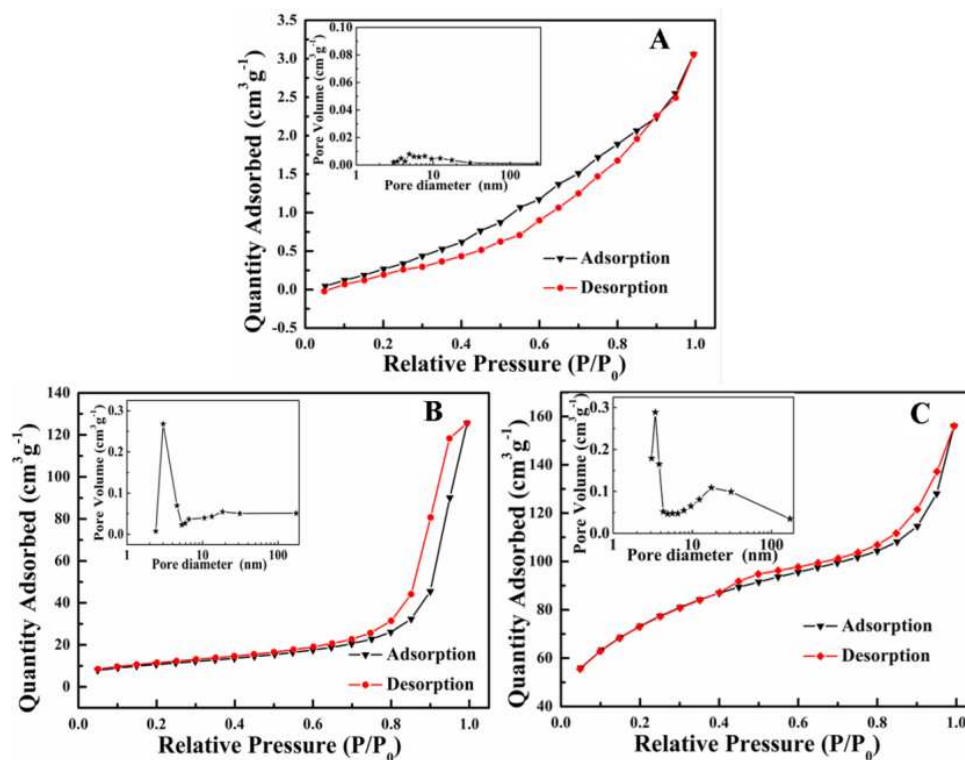


Figure 7. Nitrogen adsorption-desorption isotherms and pore size distribution of different samples (A: pristine GF; B: spherical TiO₂/GF; C: flake-like TiO₂/GF).

The nitrogen adsorption-desorption isotherms of photocatalyst are presented in Figure 7. The pristine GF exhibits a

maximum nitrogen adsorption of $3.0 \text{ cm}^3/\text{g}$ when the relative pressure reaches 1.0 (Figure 7A), and the calculated BET surface area is $6.8 \text{ m}^2/\text{g}$. A mismatch between the adsorption and desorption curves were noticed when the relative pressure was in the range of 0.2-0.9, this may result from the free volume in the sample originated from the spaces among neighboring fibres with an average diameter of $12 \mu\text{m}$. This assumption was partly confirmed by analyzing the pore volume and diameter of samples (inset in Figure 7A): the pore volume of sample is below $0.01 \text{ cm}^3/\text{g}$ irrelevant to its pore diameter, and a maximum pore volume of $0.008 \text{ cm}^3/\text{g}$ was found with pore diameter of 6 nm. For spherical TiO_2/GF composites (Figure 7B), the isotherms are of a typical type-IV pattern with H3 hysteric loops at relatively high pressures and their BET surface area reaches $78 \text{ m}^2/\text{g}^{-1}$, which is more than ten times higher than that of pristine GF. The H3 hysteresis loops suggest the presence of pores with narrow necks and wider bodies (ink-bottle pores) formed through the agglomeration of primary crystallites,³⁵ which is agreeable with SEM results (A-D in Figure 3). The pore volume (inset in Figure 7B) is much higher than that of GF, and the maximum value reaches $0.26 \text{ cm}^3/\text{g}$. The flake-like TiO_2/GF composites also exhibited a type-IV isotherm (Figure 7C), indicating the meso-porous nature of materials. The H3 and H4 hysteresis loops for this sample occurred in the relative pressure of 0.4-0.7 and 0.8-1.0, respectively, ascribing to the aggregates of plate-like particles which form slit-like pores,³⁶ quite consistent with the hierarchical structures of flake-like TiO_2/GF sample, as shown in Figure 3 E-H. The BET surface area of this sample is $251 \text{ m}^2/\text{g}^{-1}$, thanks to the micro- and nano-scale features of both TiO_2 nanoparticles and GF found in the morphology (Figure 4). The pore size distribution curve of sample (inset in Figure 7C) indicates that flake-like TiO_2/GF exhibits the highest pore volume ($0.32 \text{ cm}^3/\text{g}$) and two sharp peaks are found with pore diameter of 3.3 and 17.5 nm. Taking into account of the morphology of the sample, it seems that the former is mainly from the volume formed by the closely packed TiO_2 nanoparticle, and the latter results from the modified porous structure of GF.

3.2 Photocatalytic properties of photocatalysts

The photocatalytic activities of different TiO_2/GF samples were evaluated by the degradation of MO under UV irradiation. Figure 8A shows the UV-Vis spectra of MO at different irradiation intervals using flake-like TiO_2/GF as the photocatalyst. As displayed, the main absorption peak at 465 nm diminished gradually and disappeared after 80 min of treatment. In the meantime, no additional absorption appears in the ultraviolet region, indicating the complete destruction of aromatic structures in MO. The photographic image (inset in Figure 8) shows that the color of MO solution faded as the irradiation time increases, and it become colorless after 80 min of degradation. It should be mentioned that when the photocatalyst was incubated in MO solution, the white TiO_2/GF turned orange because of the strong adsorption of dye molecules on sample surface. Subsequent irradiation with UV light for 80 min resulted in decolorization of the MO-loaded photocatalyst, confirming the material exhibited substantial photocatalytic activity.

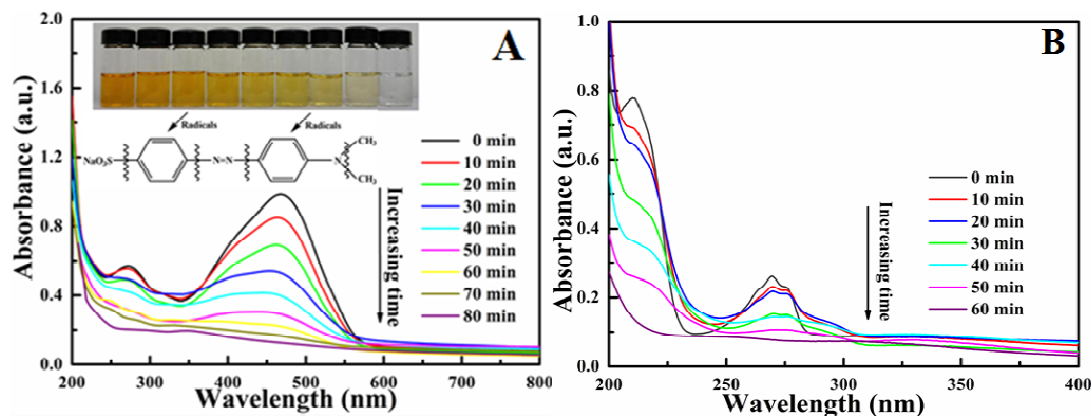


Figure 8. UV-Vis absorption spectra of MO (A) and phenol solution (B) with UV irradiation time during the photocatalytic process using flake-like TiO_2/GF (Inset A: Color of MO solution at a given time interval).

A colorless organic material, phenol, was employed as another representative model pollutant to exclude the contribution of photosensitization to the photocatalytic reaction. Figure 8B displays the temporal evolution of the spectral changes during the photodegradation of phenol over the flake-like TiO_2/GF sample, wherein the concentration of phenol was fixed at 10 mgL^{-1} . A rapid decrease in phenol absorption at a wavelength of 269 nm was observed. The sharp decrease of the major absorption band within 60 min indicates that the as-prepared flake-like TiO_2/GF sample exhibits high photocatalytic activity in the degradation of phenol, whereas the photosensitization contributes marginally to the whole photocatalytic reaction.

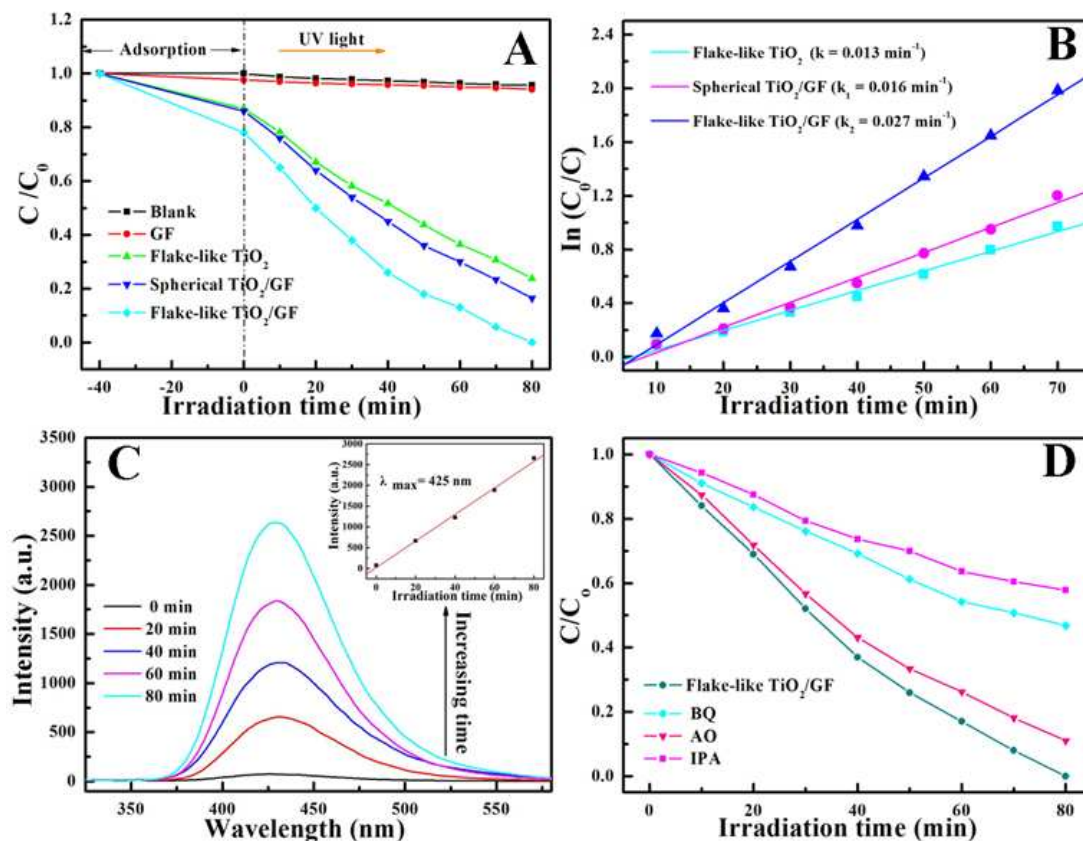


Figure 9. Evaluation on the photocatalytic performance of different materials (A: Variation of MO concentration as a function of irradiation time; B: Kinetic simulation of photodegradation process; C: PL spectral changes with irradiation time for flake-like TiO_2/GF in $5 \times 10^{-4} M$ basic solution of terephthalic acid; and D: Degradation of MO over flake-like TiO_2/GF photocatalyst with trapping agents).

Evaluation and comparison on the photocatalytic performance of different photocatalysts were conducted as well, and the results were summarized in Figure 9. Characteristic absorption peak of MO at 465 nm was employed to determine its concentration in solution, and the variation of this, i.e., C/C_0 , was plotted as a function of irradiation time over different photocatalysts, as shown in Figure 9A. Prior to the UV degradation, the solution containing photocatalyst was stirred under dark conditions for 30 min to ensure the adsorption equilibrium of dye onto the photocatalysts. MO molecule is stable and exhibits almost no decomposition in the absence of catalyst (labeled by blank in Figure 9A), therefore, its degradation by UV light is neglected here. Pristine GF also shows a similar behavior as no activity is observed under irradiation. In the presence of photocatalyst, however, the degradation of MO becomes pronounced. The difference in the adsorption ability of photocatalysts for MO may account for these different degradation processes over three samples during the initial dark irradiation. Chiefly, flake-like TiO_2/GF has a highest adsorption capacity due to its exposed porous structure along with a high surface area. Therefore, rapid decomposition of MO at the beginning (dark condition) is reasonably, and the following change with UV light could be the photocatalysis triggered by the TiO_2 with hierarchical structure on fibre surface. Flake-like TiO_2/GF exhibits relatively higher activity compared with its counterparts with spherical TiO_2/GF and flake-like TiO_2 powder: nearly 100% of MO was degraded by employing flake-like TiO_2/GF , whereas the degradation ratio for spherical TiO_2/GF and flake-like TiO_2 powder and were 83% and 74%, respectively.

The photocatalytic efficiency of flake-like TiO_2/GF photocatalyst is much higher than those of TiO_2 /activated carbon one, which generally need more than 140 min to reach comparable photocatalytic performance under the same experimental conditions.³⁸ The superior property of photocatalyst developed in this study originated from its unusual mesoporous structure as well as large surface area, which were favorable for the diffusion and separation of photo-excited charge carriers in photocatalysis.³⁹ Furthermore, surfaces and edges in nanosheets found in flake-like TiO_2/GF can serve as prominent oxidation and reduction sites for photocatalysis because they render a very short path for the diffusion of photogenerated holes and electrons on the materials. This makes the holes readily reach the surface of the materials and be trapped by interlayer, allowing more effective transport for the reactant molecules to approach the active sites on the framework of photocatalyst. The superior activity is also attributed to the efficient charge separation at the well-matched anatase/ TiO_2 -B interface, allowing photogenerated electrons and holes to readily migrate across the interfaces. Since the holes in

photocatalyst migrate much faster than excited electrons, more holes migrate to TiO₂-B and thus leads to an efficient charge separation by minimizing electron-hole recombination.²³ Therefore, the azo bond-rupture process of MO molecules is accelerated, and the subsequent cleavage of the aromatic chromophore is significantly promoted as well (Inset in Figure 8), leading to an enhanced photocatalytic activity for the photocatalyst.

To have a better understanding on the degradation kinetics of MO, the experimental data are fitted by a pseudo-first-order model, as shown in Figure 9B. Time dependent natural logarithm concentration plots ($\ln(C_0/C)$ vs. t) confirmed that the kinetics of photodegradation followed the first order behavior in good agreement with a Langmuir-Hinshelwood theory.⁴⁰ The higher the rate constant (k) value is, the faster the MO concentration decreases, and the more efficient is the photocatalytic activity of sample. The obtained k value for flake-like TiO₂/GF photocatalyst is 0.027 min⁻¹, much higher than those of flake-like TiO₂ (0.013 min⁻¹) and spherical TiO₂/GF (0.016 min⁻¹) ones. This enhancement implies that the more active surface area and mixed crystalline phases give rise to synergic effect in the photocatalysis of flake-like TiO₂ with assistance of GF.

The photoluminescence (PL) emission spectra are useful to disclose the information regarding the transfer of charge carriers as well as the fate of electron-hole pairs in semiconductors because PL emission results from the recombination of free carriers. Figure 9C shows the changes in PL spectra of terephthalic acid solution under UV irradiation at different irradiation intervals. A gradual increase of PL intensity at 426 nm occurred for the as-prepared flake-like TiO₂/GF photocatalysis (Inset in Figure 9C), suggesting the chemical reactions between the terephthalic acid and •OH species generated during the photocatalytic reaction.

Trapping experiments were performed to determine the main active species during the photocatalytic process (Figure 9D). The degradation efficiency of MO is decreased slightly upon addition of ammonium oxalate (AO, a scavenger for hole radicals), suggesting that holes are not the main active species for the degradation of MO. However, once benzoquinone (BQ), a scavenger for superoxide radicals O₂^{•-}, is added to the reaction system, the degradation of MO is remarkably prohibited (52% degradation after 80 min), suggesting the generation of O₂^{•-} and its active role during the photodegradation of MO. In contrast, the introduction of isopropanol (IPA, a scavenger for hydroxyl radicals) in the photocatalytic reaction leads to a complete suppression of MO degradation, indicating that •OH is also a species contributing to MO degradation. These results suggest that O₂^{•-} and •OH species are the driving forces in the photodegradation of MO using flake-like TiO₂/GF photocatalyst.

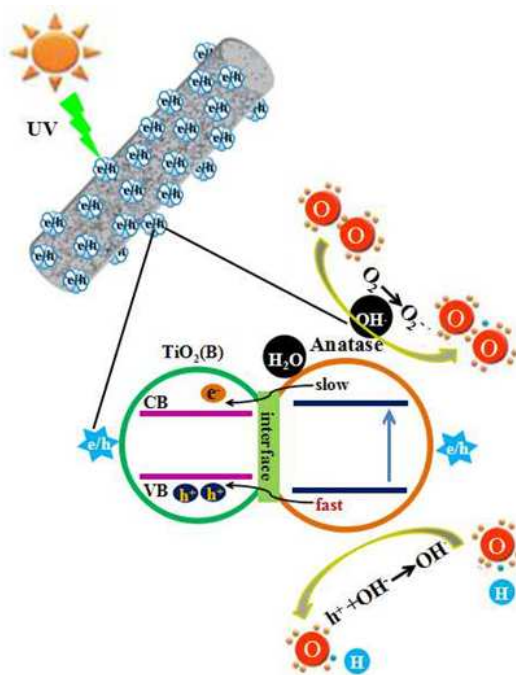


Figure 10. Schematic showing the photocatalytic process over flake-like TiO₂/GF photocatalyst.

On the basis of experimental results, a possible mechanism is proposed to explain the enhanced photocatalytic property found in flake-like TiO₂/GF, as illustrated in Figure 10. The hierarchically structured TiO₂ anchored on porous GF has several features that enhance the activity of photocatalyst, including i) Concentration enhanced photocatalysis: MO molecules in the bulk solution are condensed around TiO₂ particles by physical adsorption (Figure 9A), and a high MO concentration in the localized area is thus provided for photocatalytic reaction. The adsorption of dye on fibre surface along with the photocatalyst with efficient electron delocalization properties result in synergistic effects in improving the overall performance of flake-like

TiO₂/GF. ii) Reduced recombination of photogenerated carriers: The hetero-junction consisting of anatase and TiO₂-B phases found in flake-like TiO₂/GF promotes the photogenerated electrons and holes to readily migrate across the interfaces. Since the holes migrate much faster than excited electrons, more holes migrate to TiO₂-B and thus reduce the recombination of holes and electrons in anatase. iii) The fibrous morphology of flake-like TiO₂/GF has an additional advantage that they can be separated readily after reaction for reuse. This is very important because the high cost for the separation of photocatalyst has seriously impeded their real applications.

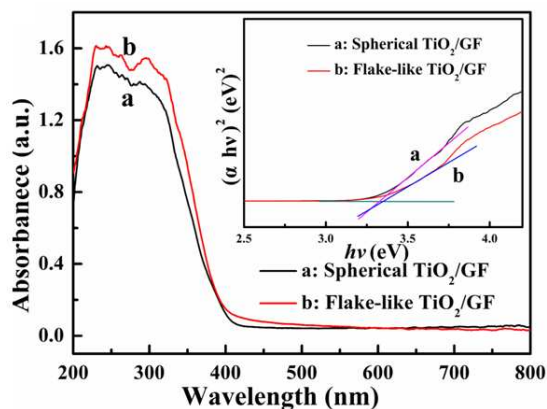


Figure 11. UV-Vis diffuse reflectance spectra of photocatalysts.

The aforementioned hypothesis was partly confirmed by measuring the band-gap of material. Figure 11 shows the UV-Vis diffuse reflectance spectra of photocatalysts and corresponding analysis on their band-gaps. The absorption onsets for both samples are at 390 nm, which is consistent with the intrinsic absorption of TiO₂. Compared with the spherical TiO₂/GF, flake-like TiO₂/GF exhibits an increased absorption in the UV region, suggesting a more pronounced interaction between the sample and UV light through the light reflection and scattering. It is widely accepted that for the photocatalyst characterized under the same experimental conditions, the higher light absorption of material has, the better photocatalytic activity exhibits.³⁷ The intercepts of plots for the optical absorption data ($[\alpha h\nu]^2$) vs. photon energy ($h\nu$) are shown in the inset of Figure 11, and the estimated band-gaps for spherical TiO₂/GF and flake-like one are 3.30, 3.33 eV, respectively. These results are higher than the band-gap of pure anatase TiO₂ (3.20 eV), possibly due to the presence of glass material in the samples. Anyway, the higher band-gaps found in the samples provide direct evidence that the possibility for the recombination of photogenerated carriers can be lowered, thus facilitate their migration with a longer life and enhance the overall photocatalytic performance of photocatalysts.

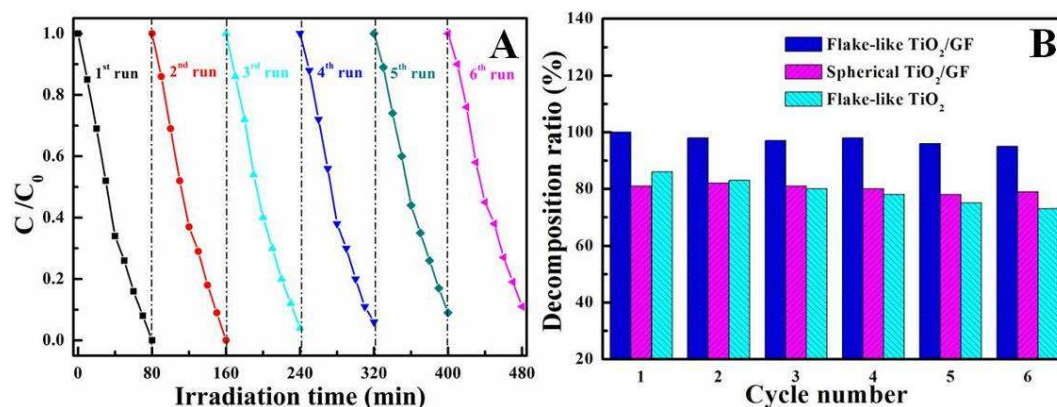


Figure 12. Cyclic photocatalytic capability of TiO₂/GF photocatalysts (A: Photocatalytic ability of flake-like TiO₂/GF under different runs; B: comparison on the decomposition ratio of MO using different photocatalysts).

The cyclic runs for the photodegradation of MO with TiO₂/GF photocatalysts were performed to evaluate their photocatalytic stability and recyclability. The change in relative degradation percentage of MO with cyclic operations using flake-like TiO₂/GF was shown in Figure 12A. As expected, this photocatalyst possesses a remarkable catalytic efficiency and recyclability. The catalytic efficiency is as high as 100% for the first cycle and remains above 89% even after six cycles, which was higher than that of spherical TiO₂/GF (decomposition ratios of spherical TiO₂/GF in the first and sixth cycle are 83% and 78%, Figure 12B). The recycle stability of flake-like TiO₂/GF was slightly lower than the spherical ones, possibly

due to the damage to the fibre substrate under alkali condition, leading to the weight loss of photocatalyst during the retrieving process. The results shown in Figure 12B also provide indirect evidence that the TiO₂ nanostructures were firmly attached on GF surface during the photocatalytic application. In addition, it also proved that the final removal of MO from solutions was dominated by the photocatalytic process rather than the adsorption one. It is worth to note that the decomposition ratio of flakes-like TiO₂ powder is the lowest one among three samples after six cycles (Figure 12B), manifesting the unique advantage of using GF in stabilizing and recycling these nanoparticles for real application. The remained high performance of the flake-like TiO₂/GF photocatalysts under cyclic runs along with their easy separation from solution guarantees their applicable and continuous photocatalysis in liquid media.

4. Conclusions

In this work, an in-situ strategy was developed to anchor TiO₂ nanoparticles on GF by the combination of solution technique and alkali hydrothermal process. Based on the experimental conditions, TiO₂ exhibited spherical or flake-like structures on fibre surface. The investigation on the photocatalytic ability of materials indicated that flake-like TiO₂/GF possessed much enhanced photocatalytic activity for the degradation of organic dye. This improvement was attributed to the large surface area of material as well as the mixed anatase and TiO₂-B phases observed in flake-like TiO₂. The combination of nanoscale TiO₂ with microscale GF offers a way to solve the problem associated with the post separation and recycle of TiO₂ photocatalysts in a slurry system, as verified by the remained photocatalytic efficiency of materials under cyclic operations. The flexible and stable TiO₂/GF photocatalyst with hierarchical structures offers more extensive possibilities for environment remediation.

Acknowledgement

This project was supported by the Western Light Program (Project No. RCPY201103) of Chinese Academy of Sciences, the 1000-Talent Program (Recruitment Program of Global Expert, In Chinese: Qian-Ren-Ji-Hua), as well as the Program for Attracting High-level Talents in Xinjiang Uyghur Autonomous Region.

References

- (1) X. Chen and S. S. Mao, *Chem. Rev.*, 2007, **107**, 2891-2959.
- (2) H. Tong, S. Ouyang, Y. Bi, N. Umezawa, M. Oshikiri and J. Ye, *Adv. Mater.*, 2012, **24**, 229-251.
- (3) S. U. M. Khan, M. Al-Shahry and W. B. Ingler, *Science*, 2002, **297**, 2243-2245.
- (4) G. R. Meseck, R. Kontic, G. R. Patzke and S. Seeger, *Adv. Funct. Mater.*, 2012, **22**, 4433-4438.
- (5) T. M. Breault and B. M. Bartlett, *J. Phys. Chem. C.*, 2013, **117**, 8611-8618.
- (6) S. Linic, P. Christopher and D. B. Ingram, *Nat. Mater.*, 2011, **10**, 911-921.
- (7) F. Cesano, D. Pellerej, D. Scarano, G. Ricchiardi and A. Zecchina, *J. Photochem. Photobiol. A*, 2012, **242**, 51-58.
- (8) J. Zhu, J. Wang, F. Lv, S. Xiao, C. Nuckolls and H. Li, *J. Am. Chem. Soc.*, 2013, **135**, 4719-4721.
- (9) Z. Zhou and M. Hartmann, *Chem. Rev.*, 2013, **42**, 3894-3912.
- (10) W. X. Guo, C. Xu, X. Wang, S. H. Wang, C. F. Pan, C. J. Lin and Z. L. Wang, *J. Am. Chem. Soc.*, 2012, **134**, 4437-4441.
- (11) M. Yang, N. Zhang and Y. Xu, *ACS Appl. Mater. Interfaces*, 2013, **5**, 1156-1164.
- (12) C. Eckerskorn, W. Mewes, H. Goretzki and F. Lottapeich, *European Journal of Biochemistry*, 2005, **3**, 509-519.
- (13) A. Piscopo, D. Robert, C. Marzolin and J.V. Weber, *J. Mater. Sci. Lett.*, 2000, **19**, 683-684.
- (14) C. H. Ao, S. C. Lee and J. C. Yu, *J. Photochem. Photobiol. A*, 2003, **156**, 171-177.
- (15) Y. S. You, K. H. Chung, Y. M. Kim, J. H. Kim and G. Seo, *Korean Journal of Chemical Engineering*, 2003, **20**, 58-64.
- (16) H. G. Yu, S. C. Lee, J. G. Yu and C. H. Ao, *J. Mol. Catal. A: Chem.*, 2006, **246**, 206-211.
- (17) M.K. Aminian, N. Taghavinia, A. Irajizad and S.M. Mahdavi, *J. Phys. Chem. C.*, 2007, **111**, 9794-9798.
- (18) X. J. Dai, Y. S. Luo, W. D. Zhang and S. Y. Fu, *Dalton Trans.*, 2010, **39**, 3426-3432.
- (19) P. Niu, L. Zhang, G. Liu and H. M. Cheng, *Adv. Funct. Mater.*, 2012, **22**, 4763-4777.
- (20) A. Y. Zhang, L. L. Long, W. W. Li, W. K. Wang and H. Q. Yu, *Chem. Commun.*, 2013, **49**, 6075-6077.
- (21) L. Chen, L.F. Shen, P. Nie, H.S. Li and X.G. Zhang, *Electrochim. Acta.*, 2012, **62**, 408-415.
- (22) A. K. Chakraborty, Z. Qi, S. Y. Chai, C. Lee, S. Y. Park, D.J. Jang and W.I. Lee, *Appl. Catal. B*, 2010, **93**, 368-375.
- (23) D. J. Yang, H. W. Liu, Z. F. Zheng, Y. Yuan, J. C. Zhao, E. R. Waclawik, X. B. Ke and H. Y. Zhu, *J. Am. Chem. Soc.*, 2009, **131**, 17885-17893.
- (24) Z. F. Zheng, H. W. Liu, J. P. Ye, J.C. Zhao, E. R. Waclawik and H. Y. Zhu, *J. Mol. Catal. A: Chem.*, 2010, **316**, 75-82.
- (25) Y. Takezawa and H. Imai, *Small*, 2006, **2**, 390-393.
- (26) R. Yoshida, Y. Suzuki and S. Yoshikawa, *J. Solid State Chem.*, 2005, **178**, 2179-2185.
- (27) A. R. Armstrong, G. Armstrong, J. Canales and P. G. Bruce, *Angew. Chem. Int. Ed.*, 2004, **43**, 2286-2288.
- (28) C. G. Silva, Y. Bouzizi, V. Fornes and H. Garcia, *J. Am. Chem. Soc.*, 2009, **131**, 13833-13839.
- (29) J. Xu, S. L. Gai, F. He, N. Niu, P. Gao, Y. J. Chen and P. P. Yang, *J. Mater. Chem. A*, 2014, **2**, 1022-1031.
- (30) J. Perez-Carvajal, P. Aranda, A. Berenguer-Murcia, D. Cazorla-Amoros, J. Coronas and E. Ruiz-Hitzky, *Langmuir*, 2013, **29**, 7449-7455.
- (31) R. J. Lu, X. Xu, J. P. Chang, Y. Zhu, S. L. Xu and F. Z. Zhang, *J. Appl. Catal. B: Environ.*, 2012, **111**, 389-396.
- (32) G. R. Williams and D. O'Hare, *J. Mater. Chem.*, 2006, **16**, 3065-3074.
- (33) C. H. Wang, X. T. Zhang, Y. L. Zhang, Y. Jia, J. K. Yang, P. P. Sun and Y. C. Liu, *J. Phys. Chem. C.*, 2011, **115**, 22276-22285.
- (34) W. J. Zhou, L. G. Gai, P. G. Hu, J. J. Cui, X. Y. Liu, D. Z. Wang, G. H. Li, H. D. Jiang, D. Liu, H. Liu and J. Y. Wang, *CrystEngComm.*

2011, **13**, 6643-6649.

(35) C. C. Tsai and H. S. Teng, *Chem.Mater.*, 2004, **16**, 4352-4358.

(36) Z. K. Zheng, B. B. Huang, X. Y. Qin, X. Y. Zhang and Y. Dai, *Chem. Eur. J.*, 2010, **16**, 11266-11270.

(37) R. J. Tayade, R. G. Kulkarni and R. V. Jasra, *Ind. Eng. Chem. Res.* 2006, **45**, 922-927.

(38) Y. J. Li, X. D. Li, J. W. Li and J. Yin, *Water Res.*, 2006, **40**, 1119-1126.

(39) G. Liu, L. Wang, H. G. Yang, H. M. Cheng and G. Q. Lu, *J. Mater. Chem.*, 2010, **20**, 831-843.

(40) M. N. Ghazzal, N. Barthen and N. Chaoui, *Appl. Catal. B*, 2011, **103**, 85-90.